The Water Masses of the Central North Atlantic in 1983—84

JOHN HARVEY

School of Environmental Sciences, University of East Anglia, Norwich, U.K.

MICHEL ARHAN

IFREMER/Centre de Brest, Plouzane, France

(Manuscript received 18 August 1987, in final form 17 May 1988)

ABSTRACT

Hydrographic surveys carried out in 1983–84 along both sides of the Mid-Atlantic Ridge between 24° and 53°N provide a detailed description of the well-known North Atlantic water masses with particular emphasis on their meridional distribution and zonal dissymetry. In the upper layers the dense horizontal sampling resolves the several narrow Gulf Stream extensions into the ocean interior, giving the image, in the Central Water density range, of a mosaïc of mode waters separated by fronts. At intermediate depths a vertical shear in the distributions of the Mediterranean Water and Labrador Sea Water stands out, both water masses having their lower part displaced southwards relative to their upper parts. Bottom waters containing nearly 20 percent of pure Antarctic Bottom Water are observed at 50°N in the eastern basin, in contrast with the western basin where proportions greater than 10 percent were found only south of 36°N along our section. This water mass analysis also gives indications that strong mixing occurs at several water mass boundaries: between Subarctic Intermediate Water and (i) North Atlantic Central Water, (ii) Mediterranean Water, and between Antarctic Bottom Water and the overlying waters.

1. Introduction

Temperature and salinity data collected during the IGY surveys and other Woods Hole Oceanographic Institution cruises in the decade 1954–64 have been used for many studies of water masses of the North Atlantic. These data provide good spatial coverage of the North Atlantic and are of high quality; being based on bottle samples, however, they are at discrete depth intervals, and although oxygen measurements were made on some cruises they have been little used due to calibration problems.

Basinwide hydrographic transects have reappeared in several programs since 1980, now using CTD casts at a finer horizontal resolution with more geochemical tracers analyzed. There is a hope that, when a sufficiently dense renewed dataset of the North Atlantic is obtained, its analysis through inverse techniques will considerably improve our knowledge of the general circulation of this basin. There have also been indications from recent datasets (e.g., Brewer et al. 1983; Pollard and Pu 1985) that real changes have occurred in the characteristics of some of the deep as well as upper water masses in the years since the IGY surveys.

The TOPOGULF CTD surveys (Fig. 1) carried out in 1983–84 contribute to this new sampling but also had their specific objectives, of which the main one was to estimate the eastward transports of mass and properties above the Mid-Atlantic Ridge (MAR). Some such computations have already been done (Sy 1988). Another particularity of the program lies in the quasi-meridional sections it provides on both sides of the MAR between 24° and 53°N. Meridional sections, though by far less numerous than zonal ones, have in the past made substantial contributions to our knowledge of the distribution of water masses in the Atlantic (Wüst 1935; Bainbridge 1980). Our sections, though clearly of more limited scope than those from the *Meteor* or GEOSECS expeditions intended to describe the global scale, are nevertheless similarly propitious to water mass studies. Owing to a better horizontal resolution they appear as detailed views in their latitudinal range, allowing there an accurate description; this is the purpose of the present paper.

The major North Atlantic water masses were sampled during TOPOGULF, as may be seen from the composite θ–S diagrams (Fig. 2), which may be compared with those published by Wright and Worthington (1970), although they should not be treated as a volumetric census as stations were not spaced uniformly and observations did not extend to the bottom at all stations. The water masses and their varieties are described below using temperature, salinity, dissolved

Corresponding author address: Dr. John Harvey, School of Environmental Sciences, University of East Anglia, Norwich NR4 7TJ, United Kingdom.
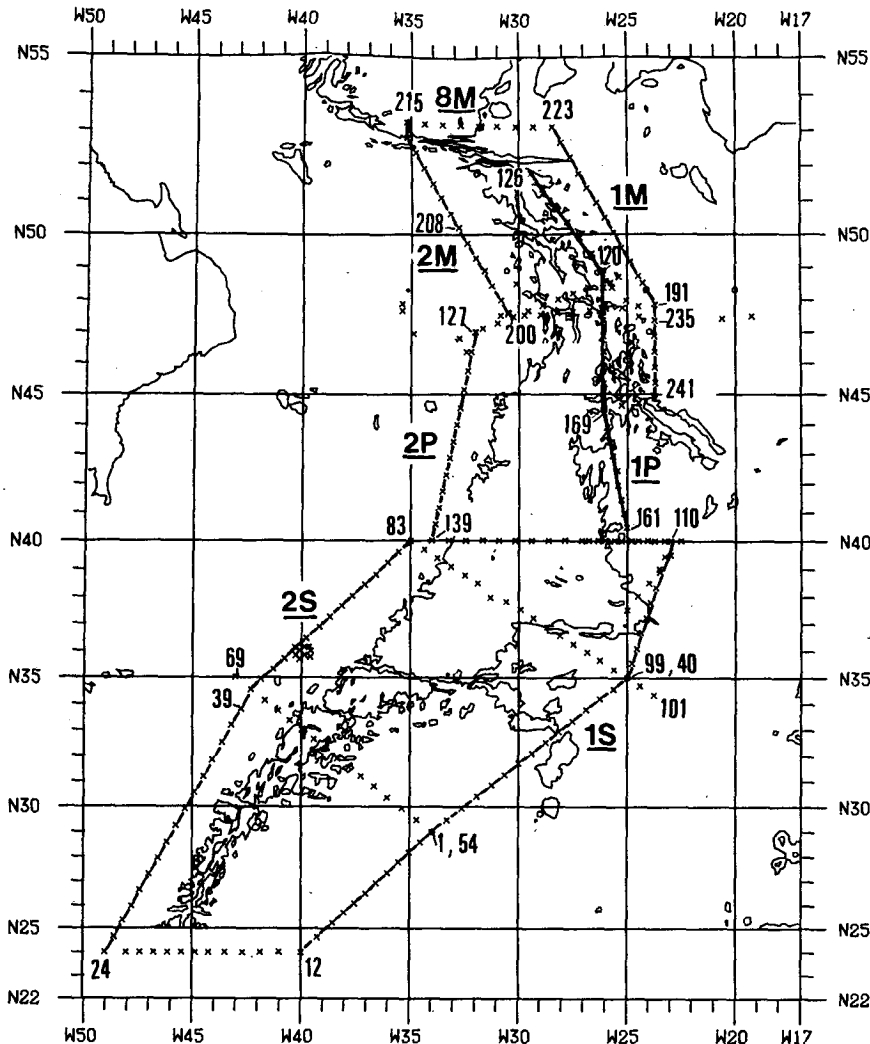
FIG. 1. The TOPOGULF CTD station grid. The sections 1S, 1P, 1M on the eastern side of the ridge, 2S, 2P, 2M on the western side, and the northernmost transverse section 8M, are indicated. The topographic contour is 3000 m.

oxygen, and large scale potential vorticity, together with nutrients for the characterization of water of southern origin. The analysis mainly rests on the examination of parameter distributions on isopycnal surfaces and the classical diagrams of properties versus potential temperature. While dissolved oxygen and nutrients are not conservative parameters they are useful tracers, particularly in the deep water where there is little biological activity. After a statement on the data quality in section 2, the water masses are reviewed starting from the upper ones and emphasis is put, for each of them, on those aspects which the TOPOGULF sections either reveal or make clearer; one of these concerns the meridional distribution of properties, and the part played by the mostly zonal major fronts of the North Atlantic (Azores front and branches of the North Atlantic Current) as separators of water masses or water

mass varieties. Another one is the west–east dissymmetry of deep and bottom waters.

2. The data quality

The TOPOGULF CTD–Tracer dataset has been reported by the TOPOGULF Group (1986). Briefly, data to 4000 db (or near bottom) were acquired from 115 stations between 24° and 40°N from Le Suroit during July to September 1983 using a Neil-Brown CTD-O_2 probe with samples for nutrient measurements being taken at 49 of these stations; data to 3000 db (or 2000 db at some stations) were acquired from 75 stations between 37°30' and 52°N from Poseidon during September and October 1983 using a Multisonde–CTD probe with samples for oxygen titration at all stations; and data to near bottom were acquired from 60 stations
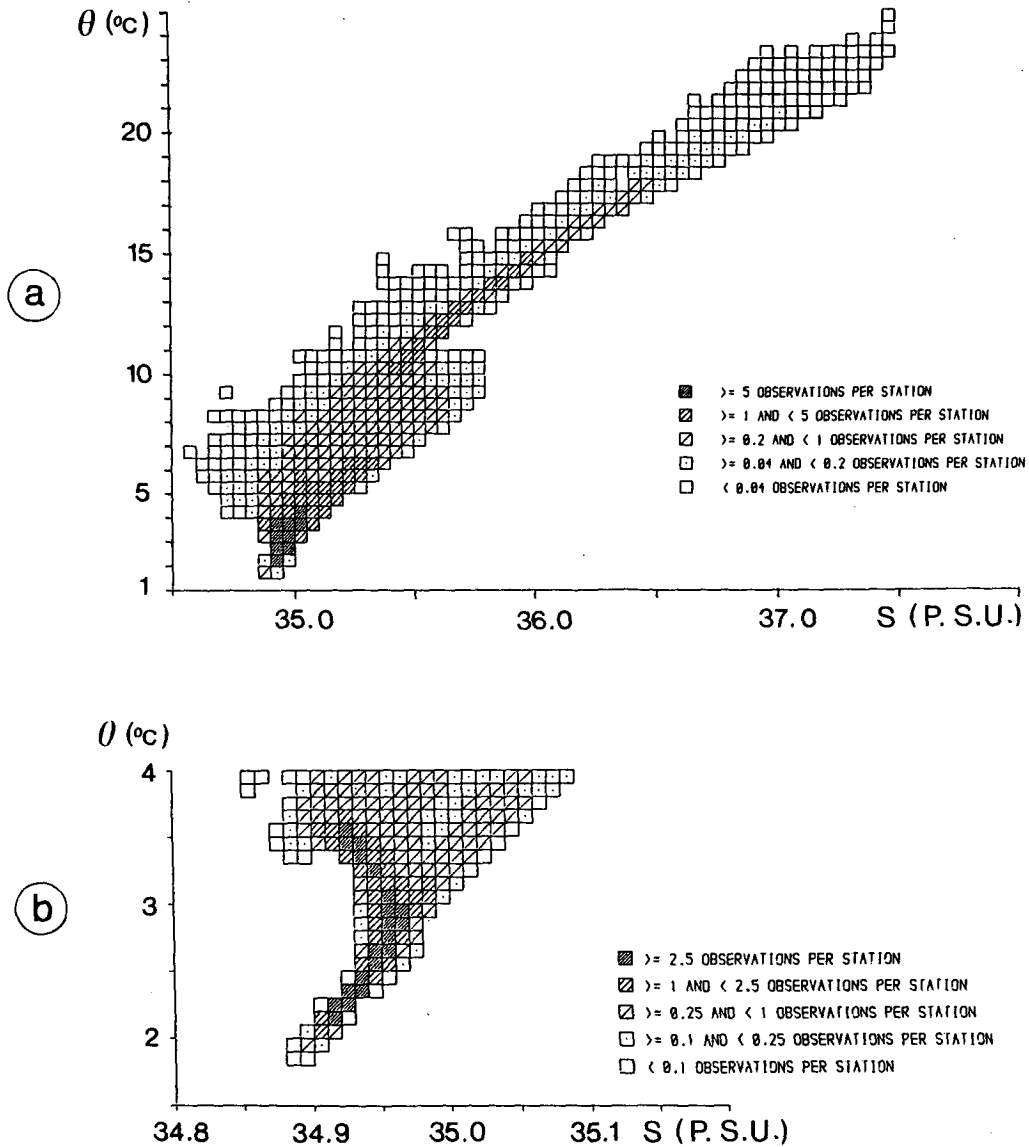
FIG. 2. (a) θ–S census for 245 TOPOGULF stations: frequency of observations at 10 db intervals, excluding data within 70 m of the surface, occurring in each bivariate θ–S class. (b) as in (a) but for water colder than 4°C only.

between 44° and 53°30'N from *Meteor* during July and August 1984 again using a Multisonde–CTD probe, with samples for oxygen titration and nutrient measurements being taken at 53 of these stations. The station spacing ranged from 35 to 50 n mi for the three ships. The data from *Le Suroit* are considered to be accurate to within 0.005°C, 1 db and 0.003 psu, and to better than 0.1 ml l^{-1} oxygen, while those from the Multisonde–CTD probe are considered accurate to within 0.005°C, 10 db and 0.01 (*Poseidon*), 0.007 (*Meteor*) practical salinity units. Standard deviations of the individual datasets, however, are generally appreciably lower than these accuracy limits, but com-

parisons between data from different ships identified two discrepancies.

The first concerns salinity data from *Poseidon* and *Le Suroit* between 37°30'N and 40°N where values from *Poseidon* were higher in both the upper and the deep water by 0.010 (±0.005); as no reason for this difference could be found, and comparisons between *Poseidon* and *Meteor* salinities at stations between 44° and 50°N showed close agreement (±0.003), no adjustment was made to eliminate this discrepancy. The second concerns oxygen values from *Meteor* compared with those from *Poseidon* at stations between 44°N and 50°N: *Meteor* values, having a standard deviation
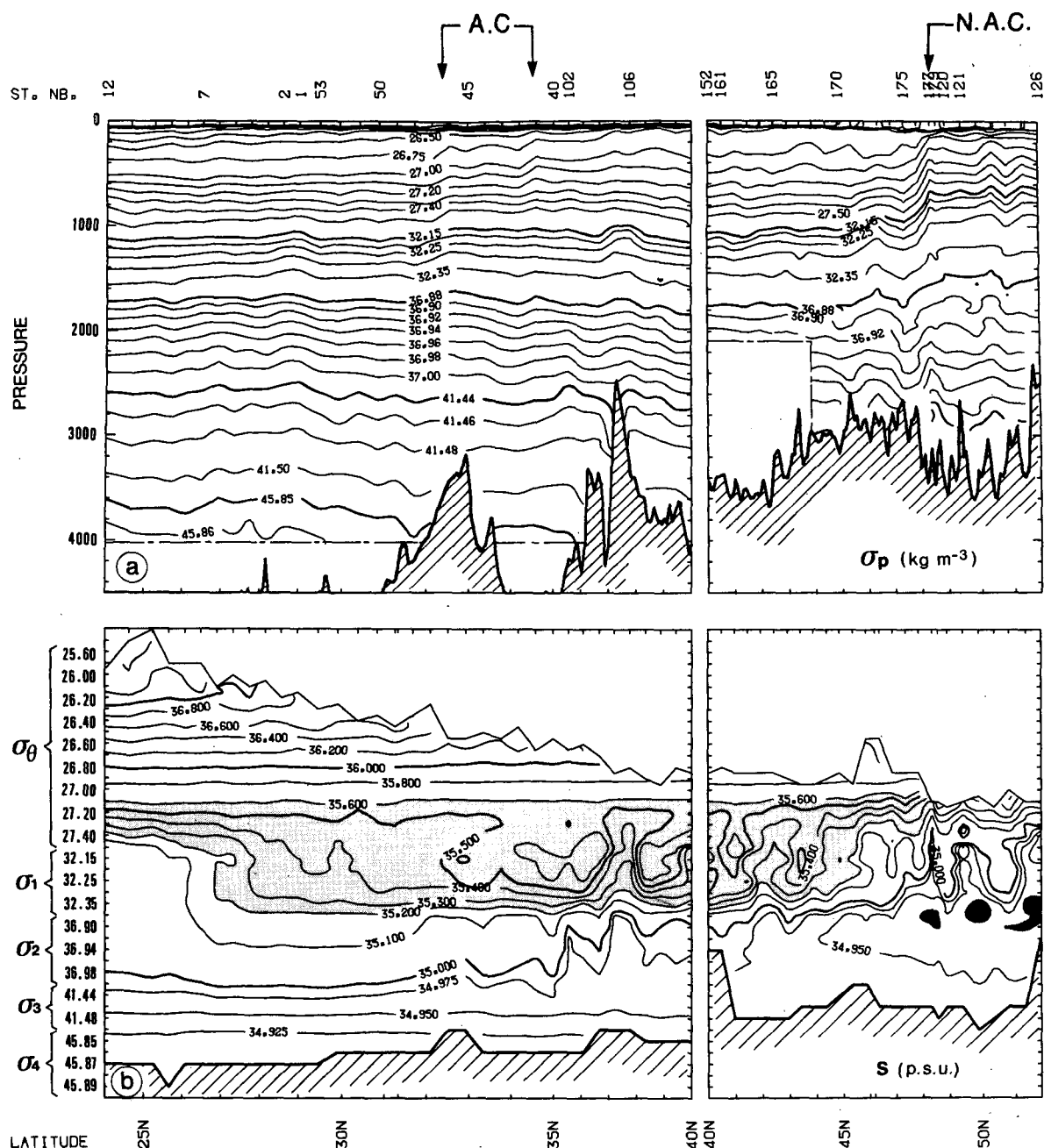
FIG. 3. Section 1S + 1P (TPG1): (a) Potential density, σ_p, vs pressure; (b) Salinity vs σ_p;
(c) Dissolved oxygen (ml l^{-1}) vs σ_p; (d) Large-scale potential vorticity, q (10^{-11} m^{-1} s^{-1}) vs σ_p.

of 0.04 ml l^{-1} were on average higher than those from *Poseidon* by about 3 percent. *Poseidon* values, while having a mean error of ±0.15 ml l^{-1} showed no consistent difference from *Le Suroit* values at stations between 37°30' and 40°N, and average values from both these ships in the deep water of the eastern basin fitted closely to Saunders (1986) value of 5.67 ml l^{-1}. Although interannual variability may affect the properties of the deep waters in the area close to their formation region, it is not expected to cause such differences on dissolved oxygen. Also, oxygen values from *Meteor* at pressures greater than 3800 db in the eastern basin at

latitudes less than 50°N, exceeded Saunders value by 2.9 percent. For these reasons a factor of 0.97 has been applied to all *Meteor* oxygen values. (It should be noted that only in this respect do the data used here differ from those presented by the TOPOGULF Group, 1986).

The nutrient data, as presented by the TOPOGULF Group (1986) were considered in the case of *Le Suroit* measurements to have precisions of 1% for phosphate and silicate values, and 1 to 2% for nitrates with a possible further error in the silicate values of up to about 1 µmol l^{-1} associated with polymerization. Replicated
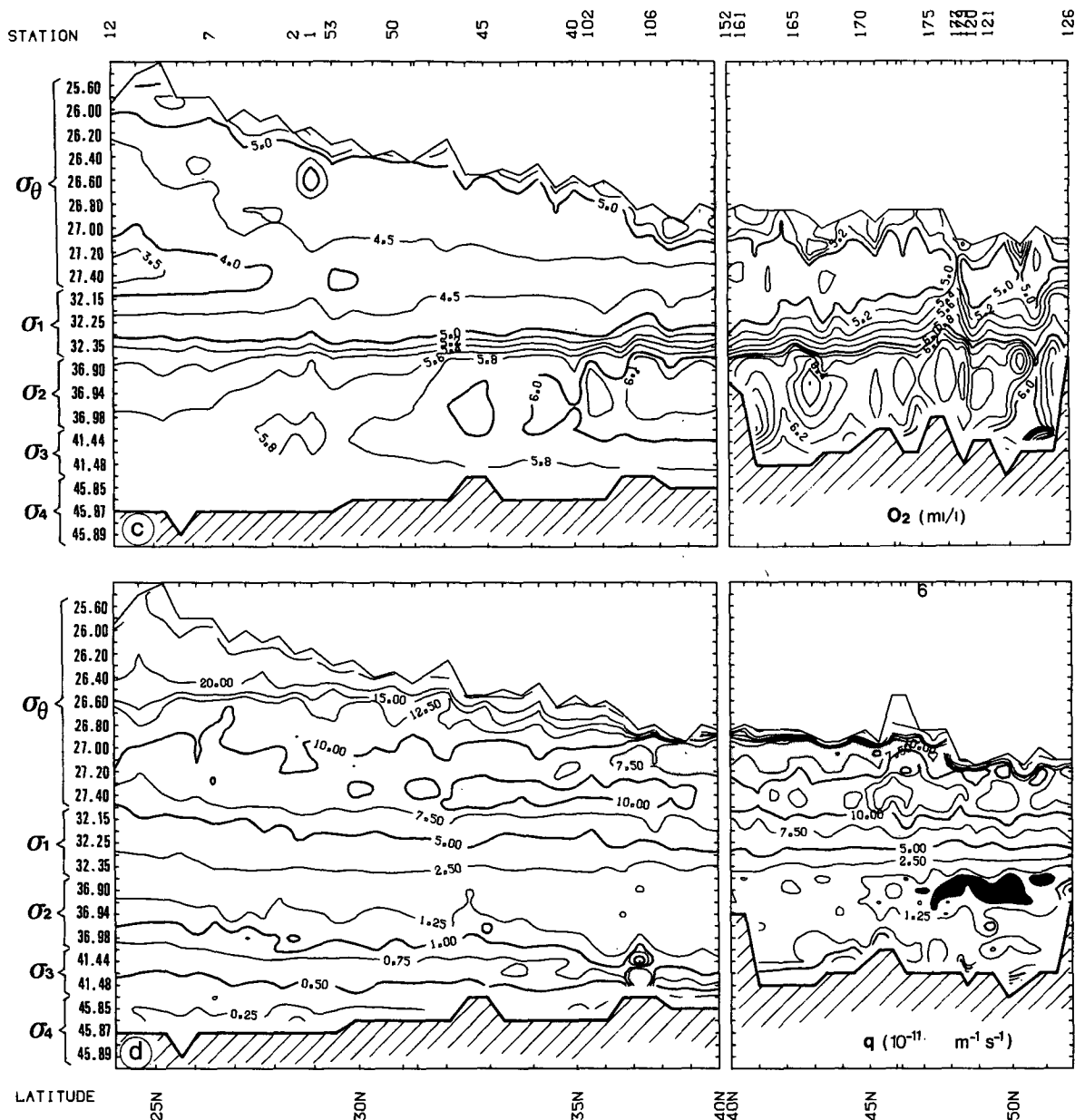
FIG. 3. (*Continued*)

nutrient samples taken by *Meteor* showed coefficients of variation of 1.1% for nitrate, 2.6% for phosphate and 3.3% for silicate.

3. The quasi-meridional vertical sections

The TOPOGULF CTD sections are identified from their numeration (Fig. 1) to which is added one of the suffixes S, P and M, respectively referred to *Le Suroit, Poseidon* and *Meteor*. We call TPG1 (resp. TPG2) the long quasi-meridional transect, combination of sections 1S and 1P (resp. 2S, 2P and 2M). Figures 3 and 4 show

the density sections and distributions of salinity (*S*), dissolved oxygen (O_2), and large scale potential vorticity (*q*) at density levels along these lines. Section 1M, which overlaps section 1P over the latitudinal range $45°-52°N$ will be presented later in Fig. 7. Properties were computed at 60 potential density levels, 40 of them being σ_θ values, and 20 values of potential density referred to 1000 db, 2000 db, 3000 db and 4000 db (resp. σ_1, σ_2, σ_3, σ_4).

Figures 3a and 4a provide the link between the pressure and density scales and confirm that no intersection of isopycnals occurs at the change from one reference level to another. They show the horizontal density gra-
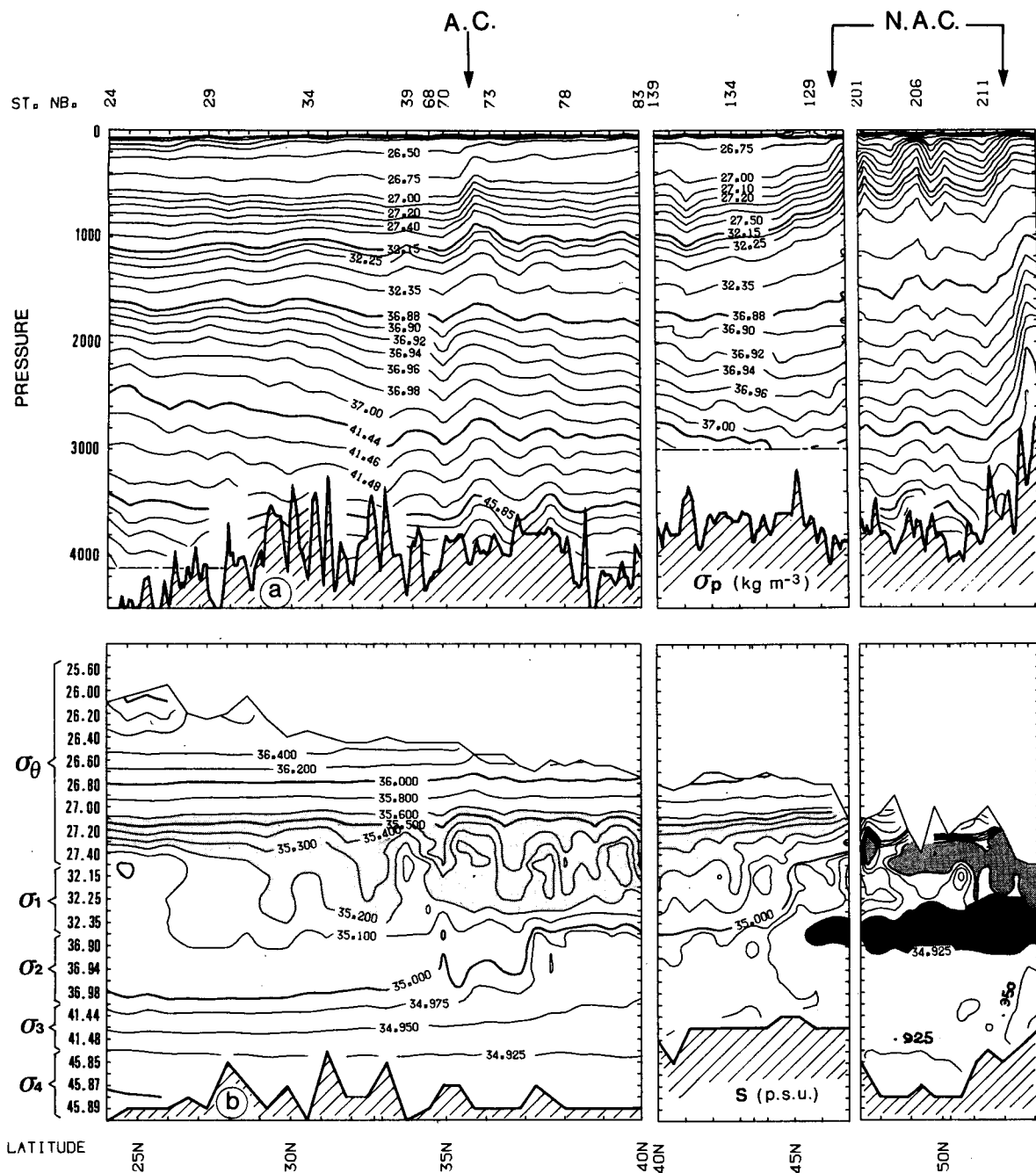
FIG. 4. As in Fig. 3 but for section 2S + 2P + 2M (TPG2).

dients, but no conclusion on the vertical density gradients should be drawn from them, due to nonuniform density steps.

The salinity, large scale potential vorticity, and dissolved oxygen south of 40°N were computed from the CTD–O$_2$ data. The potential vorticity was estimated from its relation to the Brunt–Vaïssala frequency N, $q = fN^2/g$, f being the Coriolis parameter and g the acceleration of gravity. North of 40°N the oxygen was interpolated at the density levels from the water sample values. Some smoothing of the original profiles was necessary to eliminate features of small vertical scale

from the plots. This was performed on salinity and oxygen by taking centered means over 30 db in the range $\sigma_\theta < 27.5$, and over 60 db in the range $\sigma_\theta > 27.5$, different widths having been chosen on account of the different scales above and below the main pycnocline. The potential vorticity signal was noisier, being computed from the vertical derivative of density, and was therefore more heavily filtered: centered means over 100 db were used throughout the water column for this parameter.

Matching of the parts of the sections carried out by different ships is generally satisfactory, and allows their
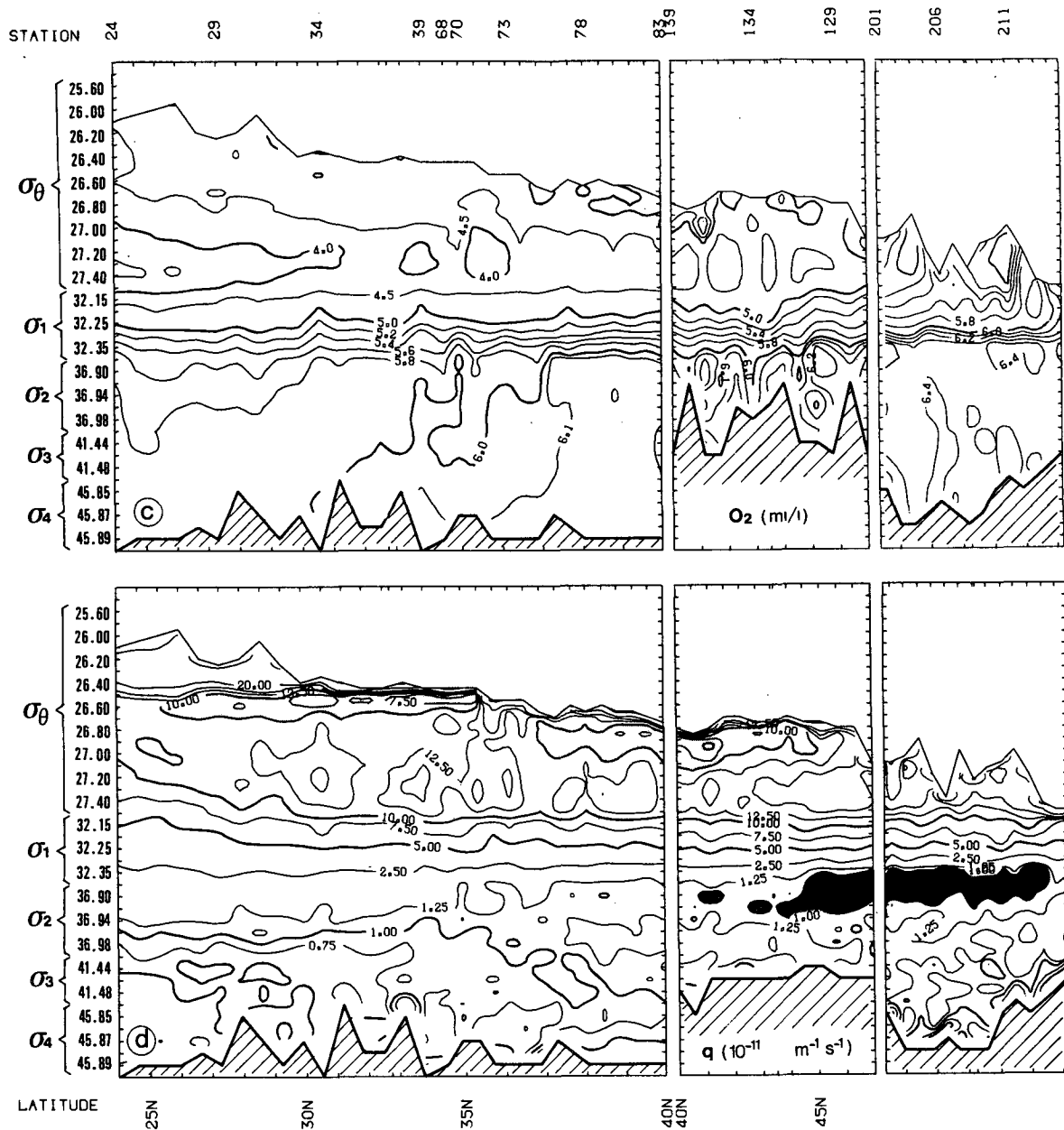
FIG. 4. (*Continued*)

nonsynopticity to be disregarded for the purpose of the present water mass analysis. Although the poor internal consistency of the *Poseidon* oxygen values is apparent at the deep levels of sections 1P and 2P, these sections are shown because of a better signal to noise ratio at the upper levels.

In order to display the property distributions at density levels (Figs. 3b, c, d and Figs. 4b, c, d) the vertical axis of the sections was graduated linearly with respect to the density index (1 to 60, with a scale twice larger above 40), the real density scale being superposed afterwards. The σ_θ isopycnals occupy half of the density

axis although they are confined to the upper 1000 db (Fig. 3a and Fig. 4a). This enhanced resolution of the upper levels, a combined result of our choice of isopycnals and density scale, was necessary for a correct visualization of the upper structures.

As our study concerns the ocean interior, the seasonal thermocline was excluded by not displaying the domain where q is greater than 50×10^{-11} m^{-1} s^{-1}. The upper limit thus defined occurs at pressures between 100 and 150 db over most of the TOPOGULF area. The lower limit shown on the sections is the first isopycnal not reached by the observations.

4. The North Atlantic Central Water (NACW)

The NACW is identified on salinity sections 3b and 4b from its quasi-horizontal isohalines generally found at $\sigma_\theta \leqslant 27.2$, south of $47°–48°N$. The density range is slightly different south of $27°N$ where it is rather $26.3 \leqslant \sigma_\theta \leqslant 27.4$. Figures 3a and 4a show the northward rise of the NACW isopycnals to occur in a series of steps rather than progressively. The steps observed in TPG1 at station pairs 46–47 and 41–42 are branches of the Azores Current and that between stations 175–177 the North Atlantic Current (NAC); these are the Gulf Stream extensions into the ocean interior. The NAC system, associated with the polar front, separates the NACW, in the south, from the Subarctic Intermediate Water (SAIW), characterized by salinities lower than 35.0 psu. As the near-surface salinities are well above 35.0 psu in the northernmost region of TPG1, another branch—at least—of the NAC certainly existed north of $52°N$ when the CTD transect was carried out. The steplike rise of the isopycnals also stands out from Fig. 4a, the Azores front being more pronounced west of the ridge, but limited to a single branch at the station pair 71–72. There are indications of an eddy to the northeast of the front, perhaps causing its intensification. Another front is visible at the northern end of section 2P at stations 127–128: this is again the southern branch of the NAC. Section 2M, carried out one year later, shows another sharp density gradient at stations 211–213. Surface salinities north of that front being lower than 35.0 psu, this is the northern branch of the polar front. The southern branch was found during the *Meteor* cruise in the zonal transect from stations 191 to 200 (Fig. 1), i.e., it intersected TPG2 south of $47°N$, close to its location on section 2P. This near coincidence may be fortuitous for the NAC system is known for its high variability (Richardson 1983; Krauss and Käse 1984), but it allows TPG2 to be treated as a synoptic transect for the purpose of the present description.

In this study we identify the southern NAC branch as the northern limit of "pure" NACW, characterized by horizontal isohalines on Figs. 3b and 4b (i.e., by a tight σ_θ relationship). Similarly we identify the northern NAC branch as the southern limit of outcropping SAIW. These branches, and the neighboring positions of the southern one in both the 1983 and 1984 surveys, are confirmed by the geostrophic computations of Sy (1988, his Fig. 12). Water with density less than 27.2 existing north of the southern branch shows salinity variations along isopycnals indicative of a looser θ–S relationship. It will be shown subsequently to be a mixture of NACW and SAIW, and called "modified" NACW.

· A less important surface frontal feature is observed around $27°N$ on both sections (at stations 6–7 on TPG1 and 27–28 on TPG2). South of these fronts the isohalines in the range $\sigma_\theta \leqslant 26.3$ are not horizontal.

These fronts are the northern boundary of the salinity maximum water formed by evaporation in the tropical North Atlantic and shown by Worthington (1976) to extend down to 150 m at these latitudes. The high salinity ($S > 37.0$ psu) surface waters appear on TPG1 south of $28°N$, but not so clearly on TPG2, because of deeper uppermost isopycnals (120–140 db) at stations 24 to 28.

Examination of Figs. 3c, d and 4c, d reveals several subdomains of the NACW. A potential vorticity minimum ($q < 7.5 \ 10^{-11} \ m^{-1} \ s^{-1}$) is visible on Fig. 4d, centered on $\sigma_\theta = 26.5$, between stations 27 and 71. This minimum, bounded in the north by the Azores front, characterizes the $18°C$ mode water (Worthington 1959). It is not visible on TPG1, an indication that the $18°C$ mode water domain does not extend to the eastern basin. The minimum is situated directly beneath the seasonal thermocline north of $33°N$, the latitude which Worthington (1972) quotes as the southern limit of the formation region, but has subducted below less dense layers farther south. No specific oxygen signature of the $18°C$ water is apparent from Fig. 4c, but closer examination shows oxygen on $\sigma_\theta = 26.5$ to decrease from ~ 4.9 ml l^{-1} at $34°N$ to ~ 4.6 ml l^{-1} at $27°N$, a confirmation of the subducted waters being older. On the other hand, a definite low oxygen anomaly exists south of the mode water and below it on TPG2, and in the south of TPG1. This is the signature of the eastern subequatorial oxygen minimum (Reid 1979) extending westwards from the African coast and centered around $15°N$. Reid and Mantyla (1978) studying the same feature in the Pacific ocean suggest an absence of water renewal in this region, an interpretation supported by the presence, in the ventilated thermocline model of Luyten et al. (1983), of an unventilated "shadow zone" southeast of the subtropical gyre. A cyclonic circulation, thermally forced, should prevail in this shadow zone according to Luyten and Stommel (1986). The TOPOGULF sections clearly show the shoaling to the south of the poorly oxygenated water, an expected characteristic of the shadow zone. McDowell (1982) observes this water which he calls "African Water" down to $\sigma_\theta = 27.6$, and notes the difficulty in distinguishing it from waters of neighboring S–O_2 characteristics coming from the south Atlantic and having crossed the equator west of the MAR. African Water is found in the southernmost TOPOGULF stations below the salinity maximum water discussed above.

Other regions of potential vorticity minima are found in both basins, bounded in the south by the Azores front and in the North by the southernmost branch of the NAC: this is the upper subpolar mode water of McCartney and Talley (1982) which we simply call subpolar mode water. The potential vorticity minimum is centered on $\sigma_\theta \sim 27.0$ on TPG1 and on $\sigma_\theta \sim 26.9$ on TPG2: this difference is consistent with the "late winter" outcropping lines of these isopycnals in

the eastern and western basins respectively (McCartney and Talley 1982). As was noted for the 18°C water, the q minimum of the subpolar mode water is found directly below the seasonal pycnocline in its northernmost part but is shielded from it by a density interval $\Delta\sigma_\theta \sim 0.2$ further south. An oxygen signature of the subpolar mode water ($O_2 > 5$ ml l^{-1}) is observed in the eastern basin, but not in the western.

Figure 5 shows plots of S, O_2 and ln$q$ versus θ at three individual stations representative of the different varieties of NACW. The 18°C mode water is identified at station 33 (Fig. 5a) from the minimum of ln$q$ around 200 db. There is no particular oxygen signature of the mode water at this station but the downward decrease of this parameter from 200 to 800 db is indicative of older water at greater depths. Station 24 (Fig. 5b) located west of the ridge, south of the surface front of stations 27–28, does not show such a distinct q minimum, but rather a constant value in the range 17° to 9°C (200 to 800 db). This kind of $\theta - \ln(q)$ diagram is also typical of the southern part of TPG1, east of the ridge. The regular θ–S relationship characteristic of NACW extended from 17° to 9°C at station 33. At station 24 it seems to continue above 17°C at shallow levels, but closer examination reveals a change of curvature at 17°C. This confirms that the salinity maximum water present at the upper levels at this station has θ–S characteristics slightly different from those of NACW. The regular θ–S relationship extends deeper at station 24 ($\sim$1000 m, $\sim$7°C) than at station 33.

The potential vorticity minimum of the subpolar mode water occurs around 13°C at station 169 (Fig. 5c). The NACW curve is limited to the potential temperature range 10° to 15°C, the MW influence being felt at $\theta < 10$°C ($p \geqslant 600$ db). No clear oxygen signature of the mode water is visible at this station.

The θ–S scatter diagrams in the "pure" NACW domains of TPG1 and TPG2 are presented on Fig. 6a, b. The diagrams show the slight curvature attributable to double-diffusion (Schmitt 1981), but a tight relationship stands out clearly, a little more pronounced in the eastern basin. The salinity standard deviation on $\sigma_\theta = 27.0$ is 0.016 psu along TPG1 and 0.029 psu along TPG2. The water is more saline east of the ridge, by 0.024 psu at 12.5°C, but the main difference comes from the mode waters being at different densities along these sections: at $\sigma_\theta \sim 27.0$ ($\theta \sim 13$°C) on TPG1 and at $\sigma_\theta \sim 26.5$ ($\theta \sim 18$°C) and $\sigma_\theta \sim 26.9$ ($\theta \sim 14$°C) on TPG2.

5. The Subarctic Intermediate Water

The most detailed study of the Atlantic SAIW is probably that of Bubnov (1968), who discussed its formation, submergence, and relation to the NAC system. As the *Poseidon* and *Meteor* cruises sampled the SAIW region (north of 36°N and 48–50°N in the western and eastern basins respectively, and west of 20°W, ac-

cording to Bubnov), they provide new material for a complementary study.

Bubnov (1968) emphasized the "double front structure of the subarctic zone." Two branches of the NAC exist on TPG2 (Fig. 4a), and although only one branch appears on TPG1 (Fig. 3a), we inferred from the absence of outcropping SAIW in this transect that a second one certainly existed. Section 1M (Fig. 7) provides another view across the NAC system. Two fronts stand out in Fig. 7a, at station pairs 224–225 and 227–228, with mesoscale variability further south. Examination of the θ–S diagrams revealed that the water in the density range $27.0 \leqslant \sigma_\theta \leqslant 27.3$ at stations 228 to 240 was less saline than the pure NACW, an indication that a third branch existed to the south of section 1M at the time of the *Meteor* cruise.

Subducted SAIW is evident to the south of the northernmost branch on TPG2 and section 1M as a fresh ($S < 34.9$ psu) intrusion in the density range $27.3 \leqslant \sigma_{\theta,1} \leqslant 32.25$. The SAIW influence is less pronounced in TPG1, but recognizable through a series of fresher ($S < 35.0$ psu) water intrusions in the same density range. Such a regime is also observed south of the branch at stations 227–228 in section 1M. Using the isohaline $S = 35.0$ psu in the above density range to determine the southern limit of the SAIW domain, this water mass is found North of 45°N on TPG2, and North of 51°N along TPG1 and section 1M, with isolated parcels of it still present at $\sim$48°N in the eastern basin. The greater southward extension in the western basin is consistent with Bubnov's observations.

Figure 8 presents the θ–S scatter diagram of the region of outcropping SAIW. Points from the seasonal thermocline, defined as $q \geqslant 100 \ 10^{-11}$ m^{-1} s^{-1} (above $\sim$100 db) are not reported. Although the whole region of outcropping SAIW was certainly not sampled during TOPOGULF, the following θ–S domain, encompassing the cloud of points of Fig. 8, is proposed to characterize the "pure" SAIW:

- $35.45 \leqslant S + 0.16\theta \leqslant 35.82$
- $27.3 \leqslant \sigma_\theta \leqslant 27.65$ (or $27.3 \leqslant \sigma_{\theta,1} \leqslant 32.25$)

This density range corresponds to the pressure domain $\sim$100 to $\sim$450 db.

The θ–S scatter diagram of the region where subducted SAIW is found on TPG1 is reported in Fig. 9. The corresponding diagrams for TPG2 and section 1M (not shown) are qualitatively similar, with the SAIW influence slightly more pronounced. The "pure" SAIW θ–S domain and the NACW line for the region south of the southern NAC branch, are also shown. A limiting line for the intermediate waters is defined, which connects the point at the base of the NACW to the point characteristic of Labrador Sea Water. No particular physical significance should be given to this line, which is used here as the boundary between intermediate waters mostly influenced by SAIW, on the left, and waters of dominant MW influence, on the right. The sub-
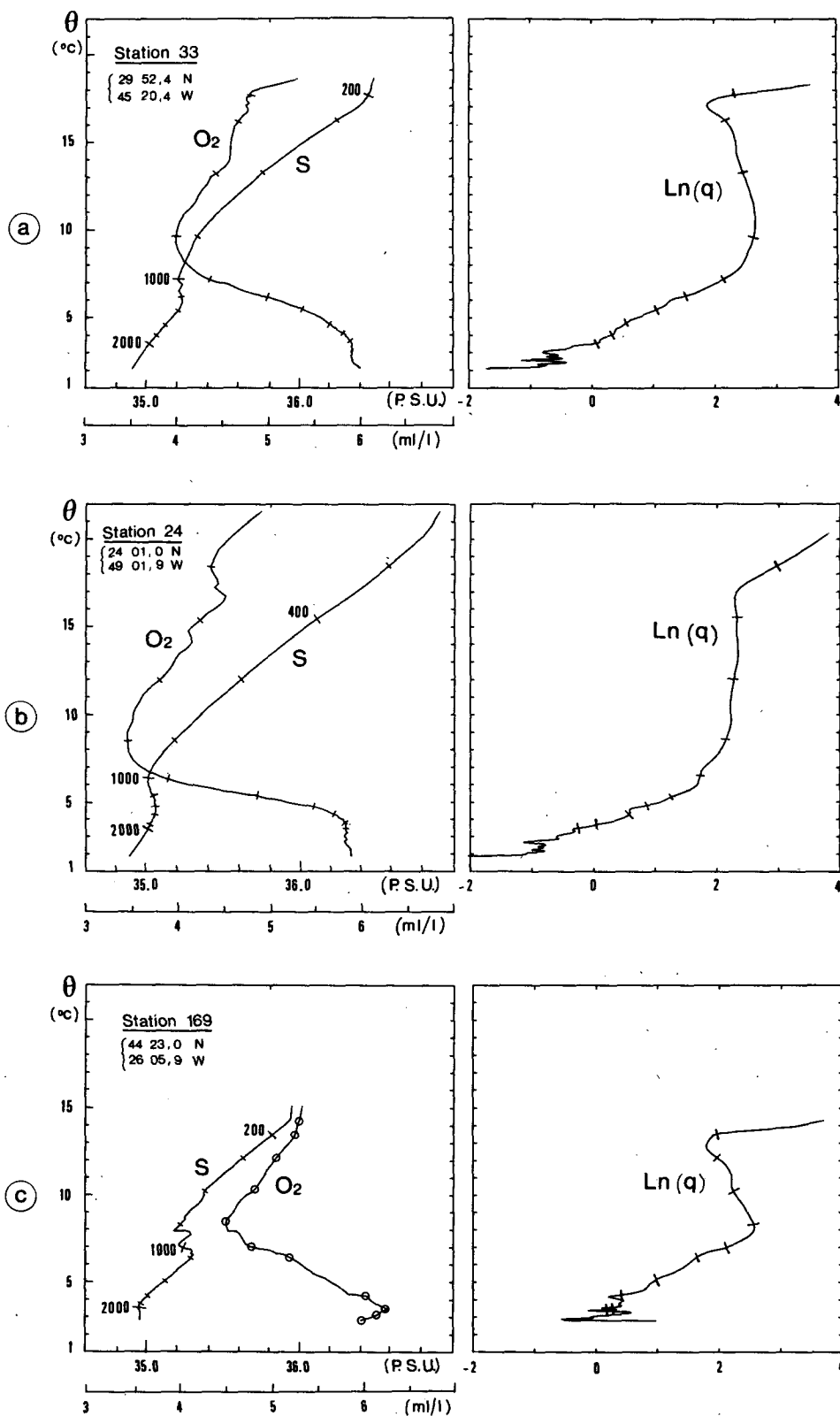
FIG. 5. S, O_2 and $\ln(q)$ vs θ for selected stations. The q unit in $\ln q$ is 10^{-11} m^{-1} s^{-1}.

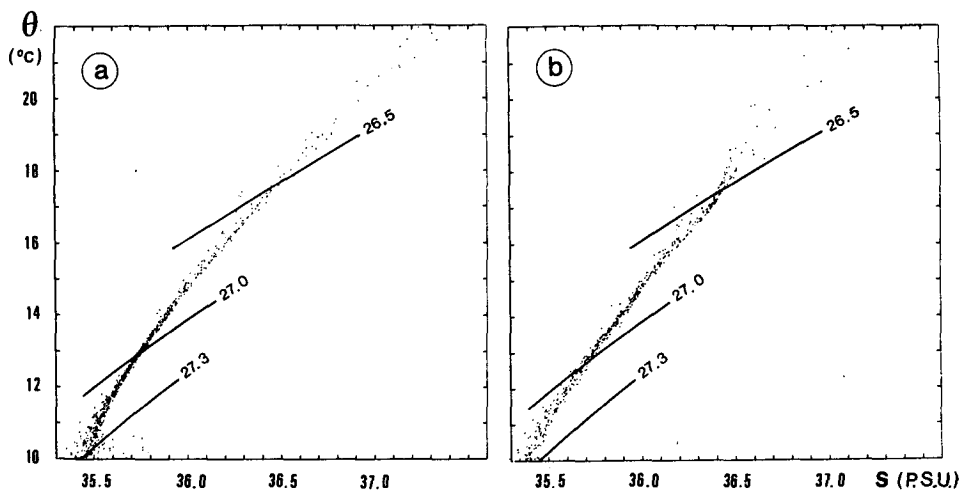FIG. 6. θ–S scatter diagrams (one point every 50 db): (a) In the eastern basin, along TPG1 south of station 176 (see Fig. 3 for the location of this station), (b) In the western basin, along TPG2 south of station 128 (see Fig. 4).
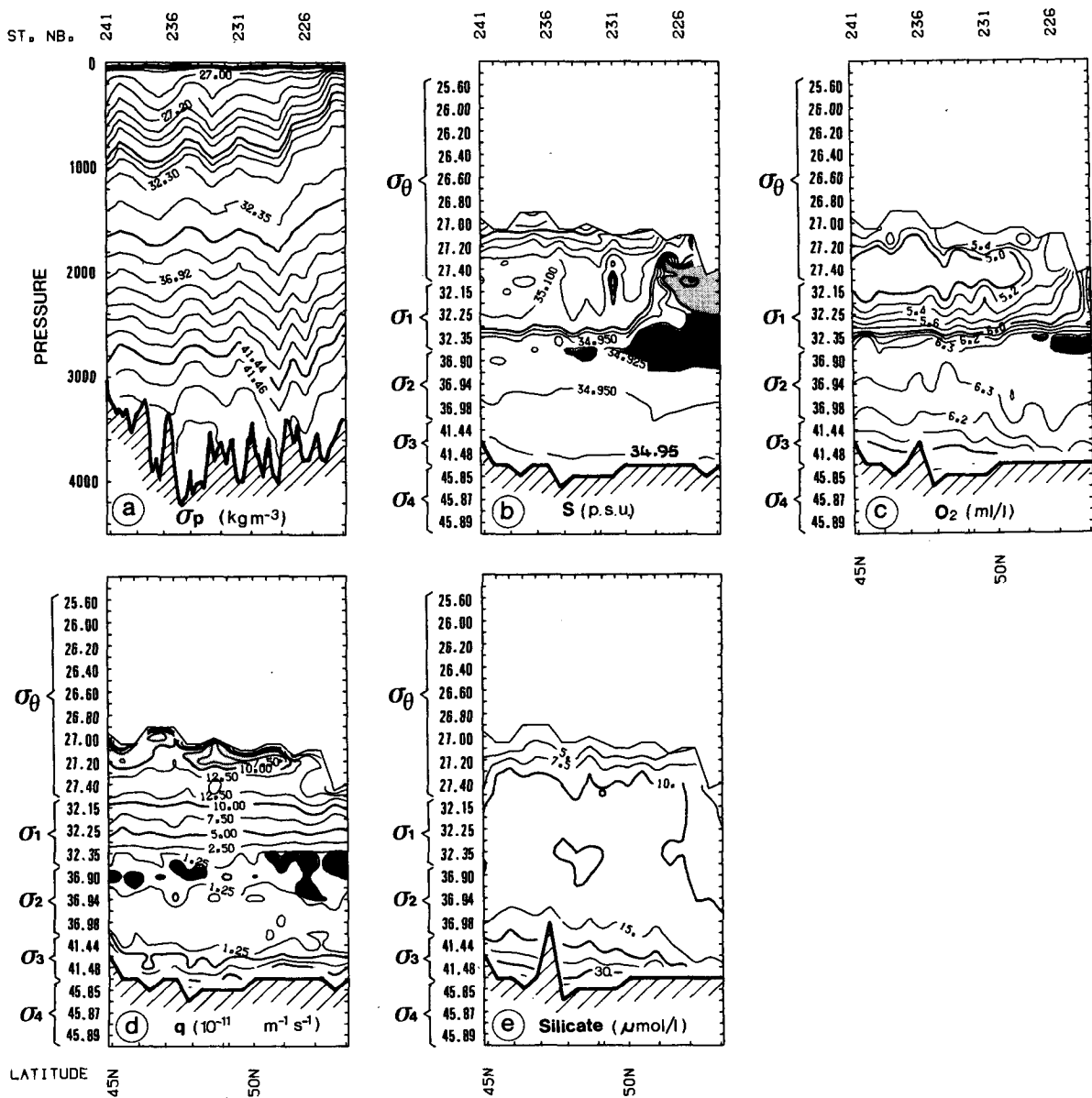

FIG. 7. Section 1M: (a)–(d) As in Fig. 3. (e) silicate (μmol l^{-1}) vs θ_p.

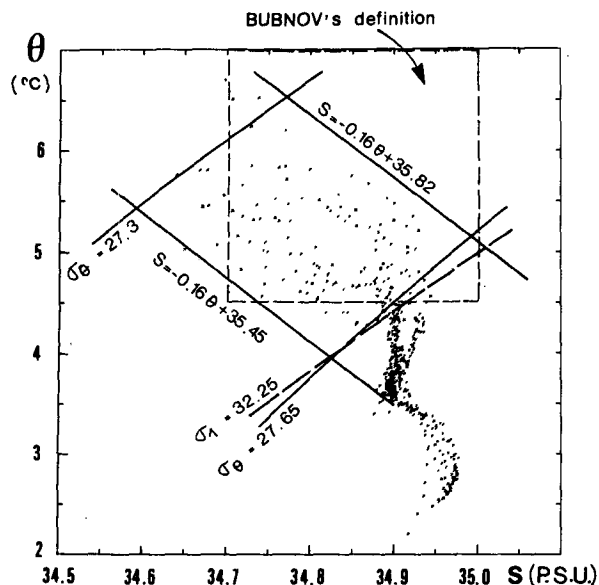FIG. 8. θ vs S for stations 213 to 224 showing definitions of SAIW.

ducted variety of SAIW is clearly more saline than the outcropping one, which suggests that either it has originated from an outcropping region other than that observed or that the "pure" SAIW has mixed with another water mass to form the subducted variety. In the latter case this other water mass could be the saline waters (MW influenced) present in the same density range farther south; such isopycnal mixing is suggested by the alternation of fresh and saline waters on TPG1 and section 1M between 45° and 51°N. Another possibility, diapycnal mixing with the overlying water mass, is suggested by the points at densities $\sigma_\theta \leqslant 27.3$ in Fig. 9, showing lower and more scattered salinities than in the region of "pure" NACW: this density level being the upper boundary of the SAIW and close to the lower boundary of the NACW, diapycnal mixing across it would cause the salinity to decrease in NACW and increase in SAIW, the observed result. The diapycnal mixing hypothesis should perhaps be favoured where the SAIW intrusion below the modified NACW is continuous, as in regions 47°–51°N of TPG2 and 51°–52°N of section 1M.

Figure 7d reveals a potential vorticity minimum ($q < 7.5 \ 10^{-11} \ m^{-1} \ s^{-1}$) around $\sigma_\theta = 27.2$ in the region of section 1M between the central and southern branches of the NAC. Patches of low potential vorticity are also observed in the same region of TPG1, but not in TPG2. As there is some tendency of the oxygen values in the same region of section 1M to be greater than 5.4 ml l^{-1}, this is likely to be a denser variety of subpolar mode water, to be encountered between the branches of the NAC, in the "modified" NACW. Figure 10 shows the θ–S, θ–O_2, and $\theta - \ln(q)$ curves at station 228 in that region: the low in potential vorticity occurs at 10°C. The closeness of the 200 and 400 db tick marks

on the θ–S curve and the high oxygen value at 10°C—though based on one single water sample—support the idea of a 10°C mode water. The diagrams of Fig. 10 and the corresponding ones in Figs. 5a and 5c illustrate three types of mode waters to be found in the North Atlantic, at temperatures around 18°, 13° and 10°. The first one is observed south of the Azores Current in the western basin; the second one between the Azores Current and the southern branch of the NAC, in both basins; the third one between the branches of the NAC, in the eastern basin.

Figure 11 displays the overall S–O_2 scatter diagram on the isopycnal surface $\sigma_1 = 32.15$, situated at the base of the SAIW. The SAIW influence is seen in the branch toward low salinity and high oxygen values: the domain $34.9 \leqslant S \leqslant 35.1$ psu, $4.8 \leqslant O_2 \leqslant 5.6$ ml l^{-1} characterizes the subducted—and mixed—SAIW, whereas the few stations around $S = 34.8$ psu, $O_2 = 6$ ml l^{-1}, are those where outcropping—and "pure"—SAIW is observed.

6. Mediterranean Water and intermediate waters of southern origin

Two further water masses are evident in Fig. 11: saline MW with oxygen content about 4.5 ml l^{-1}, and low oxygenated water with salinity about 35.0 psu. The points with anomalously high oxygen values at salinities of about 35.6 psu are from *Poseidon* stations and almost certainly result from oxygen values having been interpolated between bottle samples in the vicinity of the intermediate oxygen minimum.
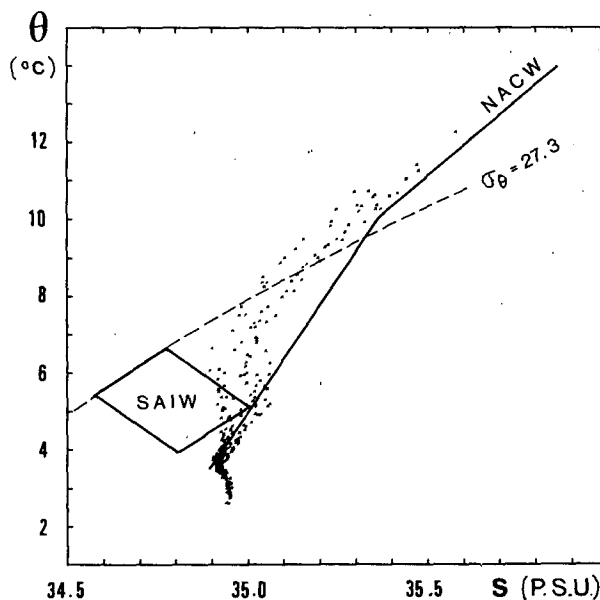

FIG. 9. θ vs S for stations 120 to 126 along TPG1 to show possible interaction between pure NACW and SAIW to form modified NACW.
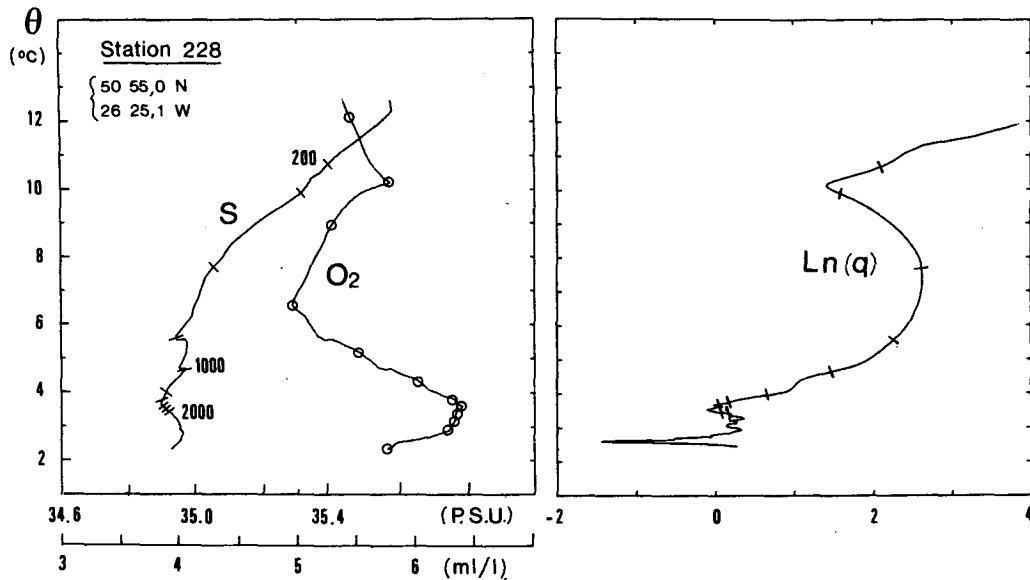
FIG. 10. S, O_2 and $\ln(q)$ vs θ for station 228 (q in 10^{-11} m^{-1} s^{-1}).

The salinity maximum which characterizes the core of intermediate MW occurs at about $\sigma_1 = 32.15$, with values in excess of 35.7 psu on TPG1 at latitudes between 30° and 40°N. North of 37°N there is considerable thermohaline mesoscale variability in this density range as higher salinity MW and lower salinity water from the north (SAIW influenced) are encountered alternately. The transition to the lower salinity water south of 27°N is more continuous. To the west of the ridge on TPG2 the salinities in the MW core are lower, generally 35.3 psu or less, and considerable mesoscale variability is evident throughout the region of MW influence. At deeper levels around $\sigma_2 = 36.9$ the salinity anomaly is highest at 28°–30°N, i.e. more than 5 degrees farther south than in the MW core above. This shift of the MW distributions at different levels may be observed in the North Atlantic atlases (Maillard 1986), but stands out most clearly in the quasi-meridional section TPG1 across the large scale MW tongue. It most probably reveals a vertical shear of the hori-
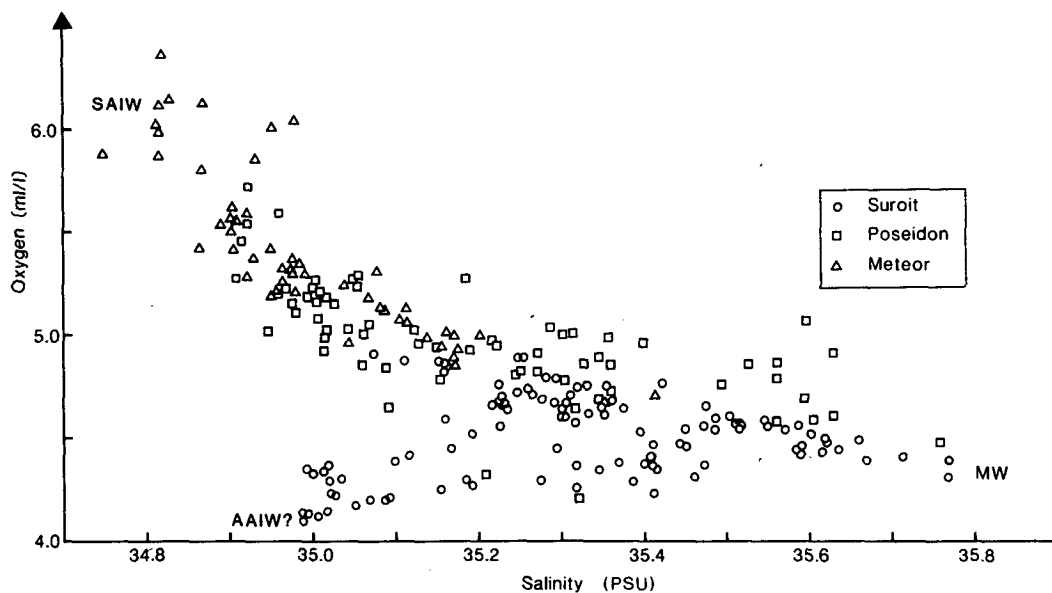

FIG. 11. Dissolved oxygen vs salinity on $\sigma_1 = 32.15$.

zontal velocities in the intrusion. Arhan (1987) suggested the dynamical effects associated with salt-fingering within the MW to be responsible for this shear.

The intermediate salinity minimum of less than 35.1 psu present in vertical profiles at stations south of about 26°30'N on both sections is within the density range $\sigma_\theta = 27.5$ to $\sigma_1 = 32.2$ characteristic of the Antarctic Intermediate Water (AAIW) found south of about 20°N in both the western and eastern basins of the Atlantic (ref. GEOSECS Atlas). Slightly lower salinity minima are encountered on TPG2 (<35.0 psu) than on TPG1, a confirmation that these minima are the signature of AAIW which McDowell (1982) shows to enter the North Atlantic West of the MAR. Although the intermediate oxygen minimum present at these stations and attributed to African Water occurs shallower ($27.3 < \sigma_\theta < 27.4$) than the salinity minimum, there is a significant vertical overlap of these anomalies and it is not evident which influence (AAIW from the west or African Water from the east) is dominant around $\sigma_1 = 32.15$ above the ridge at 24°N. The eastward salinity gradient around 1000 m is confirmed in the 24°N section of Roemmich and Wunsch (1985), associated with similar nutrient gradients. These authors suggest an eastward flow of AAIW in the tropics to feed a northward current along the African coast. As the oxygen minimum is lowest near Africa, African Water could then be partly composed of AAIW having acquired new oxygen and nutrient characteristics offshore from Africa.

7. Labrador Sea Water, deep Mediterranean Water, and deep Southern Water

We consider in this section the density range $32.25 \le \sigma_{1,2} \le 36.98$ which is occupied in the TOPOGULF area by water masses from three distinct origins: Labrador Sea Water, deep Mediterranean Water and a third water mass of less defined origin which we call Southern Water (SW). The basic part played by these water masses stands out on the S–O$_2$ scatter diagram on σ_2 = 36.88 (Fig. 12) exhibiting a clear mixing triangle. The diagram shows no mixing to occur between LSW and SW within the TOPOGULF region, these water masses being separated by MW.

The LSW is visible in the north of TPG1, TPG2 and section 1M (Figs. 3b, 4b, 7b) as a fresh anomaly centered on $\sigma_2 = 36.88$ and intruding in the ocean below the SAIW tongue. The associated vertical salinity minimum is lower than 34.9 psu on TPG2 and section 1M, and resolvable north of about 44°N. If we use the isohaline $S = 35.0$ psu as the extreme limit of influence of LSW, the upper LSW ($\sigma_2 < 36.88$) is bounded in the south at latitudes from 42° to 47°N on TPG1 and 42° to 45°N on TPG2, depending on the exact density. The lower LSW ($\sigma_2 > 36.88$) extends farther to the south particularly on TPG1 where at about 35°N there is a sharp boundary with the more saline deep MW.

In their comprehensive study of the LSW Talley and McCartney (1982) placed the southern limit of the LSW around 40°N in the Azores region, and noted that "the MW and the LSW overlap in a band more than 500 km wide along the southeastern side of the LSW core." This overlapping should be interpreted as the difference between the above limiting latitudes of the upper and lower LSW. The different behavior of the LSW at different levels may be indicative of a vertical shear of the horizontal velocity within this water mass, similar to the one observed in the MW. Another possibility is to regard the higher salinities of the upper LSW as the result of double-diffusive diapycnal mixing with the overlying MW.

The location of the southern boundary of the lower LSW allows zonal exchanges of this water mass between basins in the region south of the Azores plateau. Such a passage would be consistent with the different latitudes of this boundary on TPG1 (35°N) and TPG2 (37°N), suggesting a front parallel to the fracture zones of the MAR in that region. This front is located 90 n mi north of the Azores Current on TPG2 and 60 n mi north of its northern branch on TPG1.

A vertical oxygen maximum ($O_2 > 6.4$ ml l^{-1}) marks the core of the LSW north of 51°N on the Meteor sections. At the southern end of the LSW domain the boundary between lower LSW and deep MW is marked on the oxygen sections by a sharp step in both the 6.0 and 6.1 ml l^{-1} isolines. At intermediate latitudes the high LSW oxygen values cannot be distinguished from those of the underlying waters. A better tracer is the potential vorticity, already used by Talley and McCartney (1982): the core of the LSW is characterized on TPG1, TPG2, and section 1M by a vertical q minimum ($q < 10^{-11}$ m^{-1} s^{-1}), whose southward extension is comparable to that of the salinity minimum. Potential vorticity is also the best tracer to show the west-east dissymmetry of the LSW, the region where $q < 10^{-11}$ m^{-1} s^{-1}—within $32.25 < \sigma_{1,2} < 36.98$—being more widespread on TPG2 than on TPG1. Mapping the distribution of LSW from its q minimum, Talley and McCartney (1982) observed that three tongues emanate from the source region, one of them extending eastward across the MAR around 50°N. The closed q contours at this latitude on TPG1 must be the cross section of this branch. Section 1M was carried out some 80 n mi east of TPG1; the more diluted aspect of the LSW q anomaly along this section may reflect the eventual southward turning of the eastward branch, visible on the chart of Talley and McCartney (their Fig. 3). Considering the possibility of a passage of LSW south of the Azores, the ultimate fate of the LSW brought in the eastern basin by this branch around 50°N could be to flow back westwards into the western basin between the Azores plateau and 35°–37°N.

We call "deep MW" the saline waters found south of the LSW and north of about 27°N in the density range $32.25 < \sigma_{1,2} < 36.98$ on both TPG1 and TPG2.
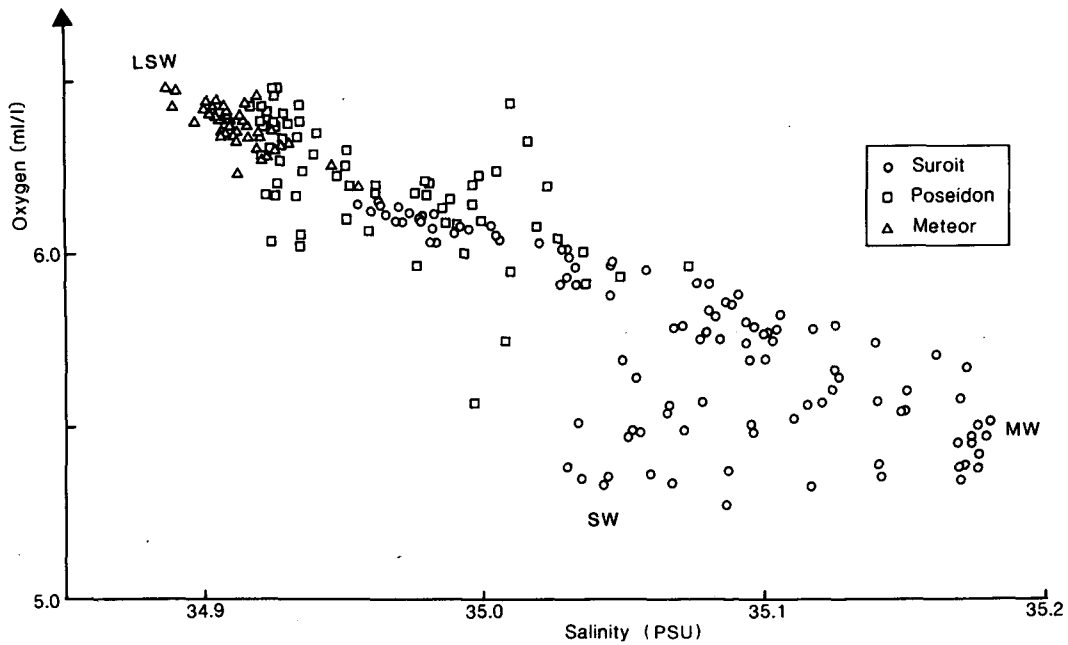
FIG. 12. Dissolved oxygen vs salinity on σ_2 = 36.88.

The corresponding pressure range is 1300 to 2300 db. The descent of the Mediterranean Current in the Gulf of Cadiz is limited by entrainment and external stratification to about 1200 m (Smith 1975) and hence most of this deep MW has probably not issued directly from the MW source but has gained its high salinity through diapycnal mixing (salt-fingering) causing a downward salt flux below the MW core. We observed in section 6 the greater southward spreading of the deep MW. Its southern boundary is shown by quasi-vertical isohalines at densities σ_2 < 36.94. This well-marked limit and the sharp northern one with the lower LSW suggest the salinity field in the deep MW to be determined by advection—and diapycnal mixing—rather than lateral mixing.

In the upper density ranges (sections 4 and 6) we noted the difficulty to separate the influences of AAIW and African water south of 27°N. We face the same problem with the low salinity water found south of the deep MW in the density range 32.25 < $\sigma_{1,2}$ < 36.94. These low salinities could be the downward extension of the AAIW signature, but examination of the North Atlantic Ocean atlas of Worthington and Wright (1970) rather suggests a southeastern origin, as salinity on θ = 3.8°C and θ = 4.0°C in this density range is lowest in the tropics along the African coast.

8. Mid-deep water

The oxygen–salinity diagram on the σ_3 = 41.44 surface (Fig. 13) suggests the influence of at least four water masses at this level, which generally occurs between 2500 and 3000 db. The two waters of high ox-

ygen content (>6.2 ml l^{-1}) are encountered in the northern part of the TOPOGULF area and may be identified as Northwest Atlantic Deep Water (NWADW, with lower salinity) and Iceland–Scotland Overflow Water (ISOW, with higher salinity). The most saline water encountered (>34.975) is between 29° and 30°N on TPG1 and must again be attributed to MW influence, while that of lowest oxygen content (<5.7 ml l^{-1}) occurs at the southern end of TPG1 and indicates the influence of water of southern origin.

In Fig. 13 ISOW is only evident (S > 34.96 psu, O_2 > 6.2 ml l^{-1}) at about ten *Meteor* stations in the vicinity of the Charlie Gibbs Fracture Zone (CGFZ) in the northwestern corner of the TOPOGULF region. Figure
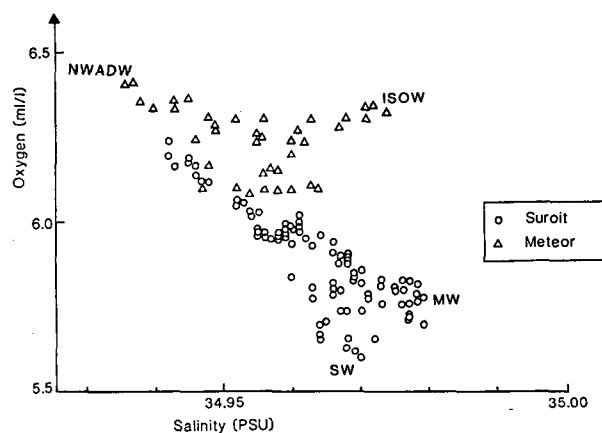
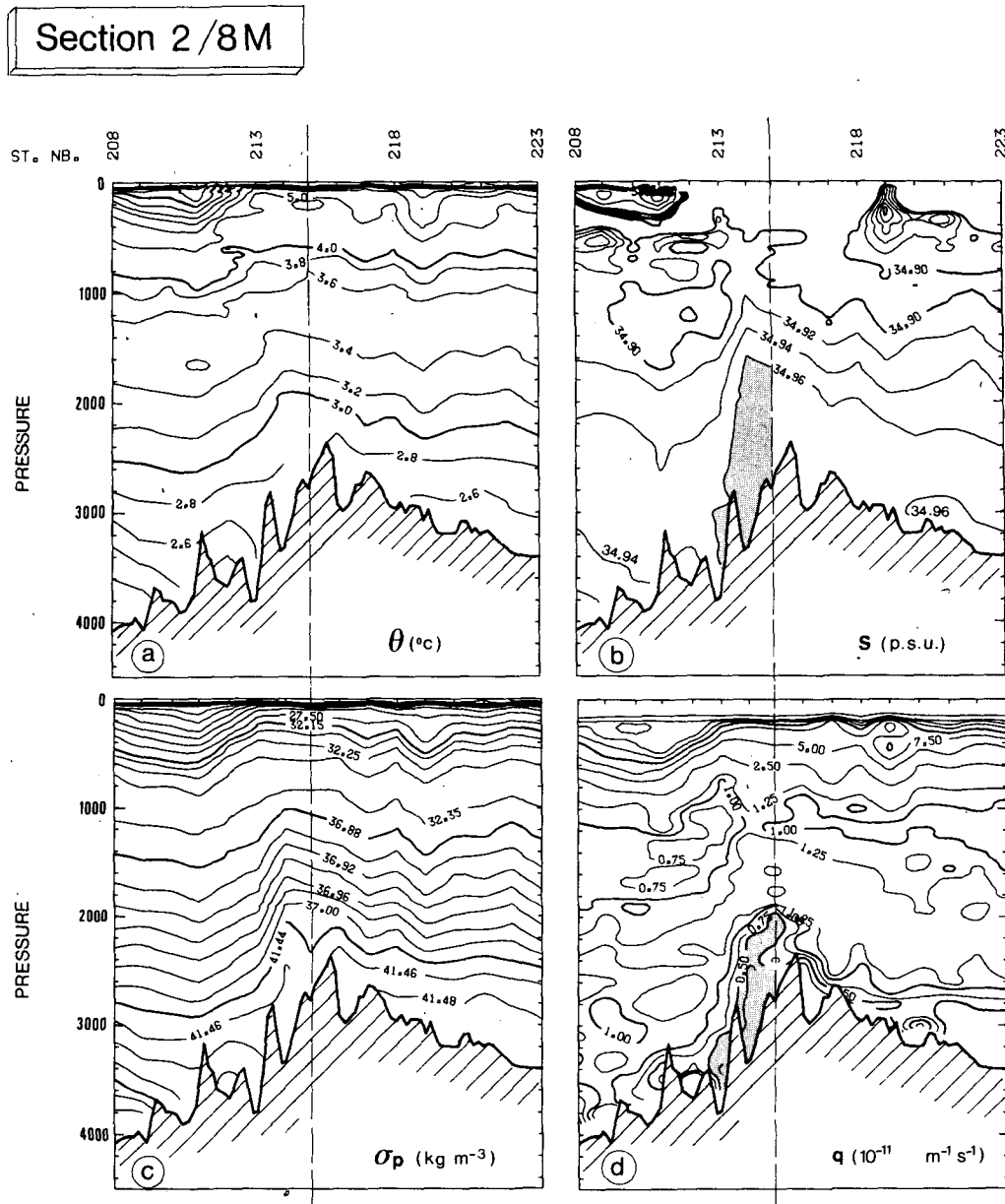FIG. 13. Dissolved oxygen vs salinity on σ_3 = 41.44.

Section 2/8M

ST. NB.

FIG. 14. Section 2/8M: (a) Potential temperature vs pressure; (b) Salinity vs pressure; (c) Potential density, σ_p, vs pressure; (d) Large-scale potential vorticity, q, vs pressure. The light broken line separates the meridional and zonal parts of the section. The shaded area shows ISOW at the outflow from CGFZ.

14 presents a section comprising that part of section 2M north of 50°N (stations 208 to 215) and the transverse section eastwards along 53°N (stations 215 to 223). Pressure is kept as vertical coordinate on this figure to better show the relation of anomalies to topography. A marked northward rise of the isopycnals occurs between 1200 and 2800 m at the station pair 213–214, while just north of this front the density gradient strongly reverses below 2000 m (see isoline σ_3 = 41.44 at station pair 214–215). It is in the vicinity of station 214, located on the northern side of the

northern trough of the CGFZ and near to its sill (Harvey 1980), that we may expect the ISOW to flow west and it is there that we indeed observe it. The southward flow which feeds the ISOW stream through the CGFZ crosses the transverse section over a wider extent, the shallower components being furthest to the west. While flowing south the core of this water is characterized by high potential vorticity, generally >1.25 10^{-11} m^{-1} s^{-1}, but where it is flowing west its potential vorticity appears to have decreased markedly so that the ISOW is characterized by minimum values of about

$0.5 \ 10^{-11} \ m^{-1} \ s^{-1}$ (shaded on Fig. 14). This apparent change may be due to a change in relative vorticity not taken into account in estimating q, or to a real change in potential vorticity associated with the passage through the CGFZ. It could also result from adjustment of the ISOW to its new environment as it enters the western basin.

An outstanding question concerns the extent to which ISOW penetrates south of the CGFZ in the eastern basin. Use of salinity as a tracer is unsatisfactory as it does not distinguish ISOW from that influenced by MW. Thus a deep salinity maximum (>34.95 psu) exists along the full length of section 1M. The salinity value in this maximum however decreases southwards to about 50°30'N (not apparent on the figure) where it occurs below 3000 db; south of this the maximum occurs at a shallower level (2750 db) and its value increases southwards to about 48°N. Oxygen content, used by Harvey and Theodorou (1986) to distinguish ISOW and MW influences, also shows a sharp southward decrease (from 6.26 to 6.14 ml l^{-1}) on the σ_3 = 41.44 surface at about 50°N. These observations indicate that along this section the influence of ISOW is greatly reduced south of 50°N and that the salinity maximum south of this latitude is largely attributable to MW influence beneath the LSW core. Data from section 1P (Fig. 3) do not extend down to the salinity maximum at all stations, and both the salinity and oxygen data from this section are less accurate than those from section 1M and have therefore been omitted from Fig. 13. Nevertheless the value of the deep salinity maximum in section 1P increases southwards from about 34.955 at 49°N to 34.975 at 42°N while the depth at which it occurs decreases from about 2900 to about 2400 db over the same latitude range, which supports the conclusions drawn from section 1M.

NWADW in Fig. 13 was found in stations south of 50°N on section 2M (west of the MAR). On section 2P salinity increases southwards at σ_3 = 41.44, suggesting a decreasing influence of NWADW relative to MW south of 47°N. This pattern is consistent with Worthington and Wright's (1970) charts of salinity on θ = 2.8° and 3.0°C, which indicate the less saline water originating in the northwest Atlantic spreading towards the MAR from the western boundary in the vicinity of Flemish Cap (about 47°N).

The region of MW influence at this level is again found well to the south of its source at 36°N, at latitudes between 27° and 30°N on TPG1 and between 25° and 30°N on TPG2.

The water of lowest oxygen content in Fig. 13 is present on the eastern side of the MAR and generally has the highest nutrient concentration, most notably phosphate, of any of the TOPOGULF water at this density level. Examination of the GEOSECS atlas supports the contention that these characteristics are attributable to Antarctic influence: they could have been advected through the South Atlantic despite the gen-

erally southward advance of North Atlantic deep waters at this level or they could result from vertical mixing with Antarctic Bottom Water below.

9. Lower-deep and bottom water

The σ_4 = 45.85 surface, occurring at pressures ranging from 3400 db in the northwest to more than 4000 db in the northeast was reached by most Le Suroit and Meteor stations south of 51°N on TPG2, but by only three stations north of 40°N to the east of the MAR. The salinity-oxygen plot on this surface (Fig. 15) exhibits most clearly the west–east dissymetry of bottom water. On the east of the ridge, with the exception only of station 17, all salinities lie within 0.002 of 34.916 psu and oxygens within ±0.05 of 5.68 ml l^{-1}. Saunders (1986) values, for comparison, are 34.915 psu and 5.67 ml l^{-1}. To the west of the ridge oxygen increases northwards, attributable to the influence of NWADW mentioned in the previous section. The higher salinity at stations 208 and 209 appears to be associated with the flow into the western basin through the CGFZ. The most likely source of the lower salinity water at station 17, situated immediately east of the ridge on the northern side of the Kane FZ, is a flow from the south with a significant Antarctic Bottom Water (AABW) component. Some of this water may reach the western basin through the Kane FZ accounting for the lower salinities at stations 22 to 26 inclusive.

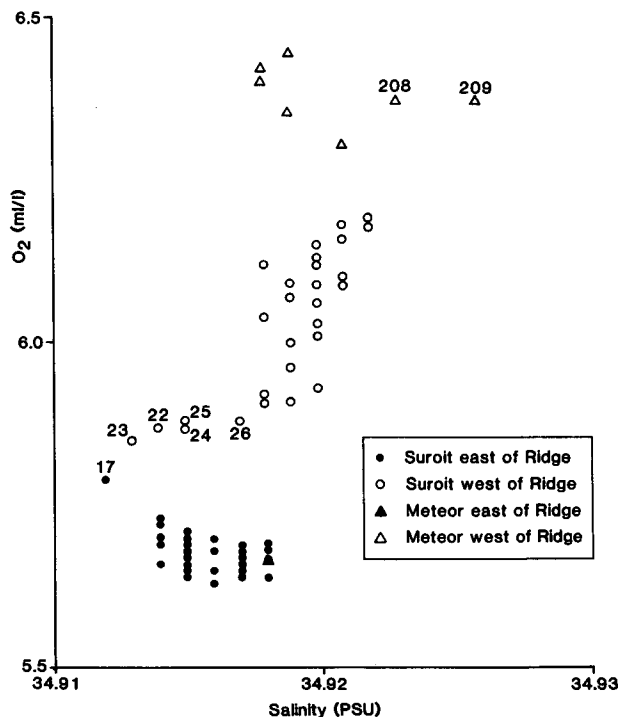In order to assess the extent of Antarctic water in-

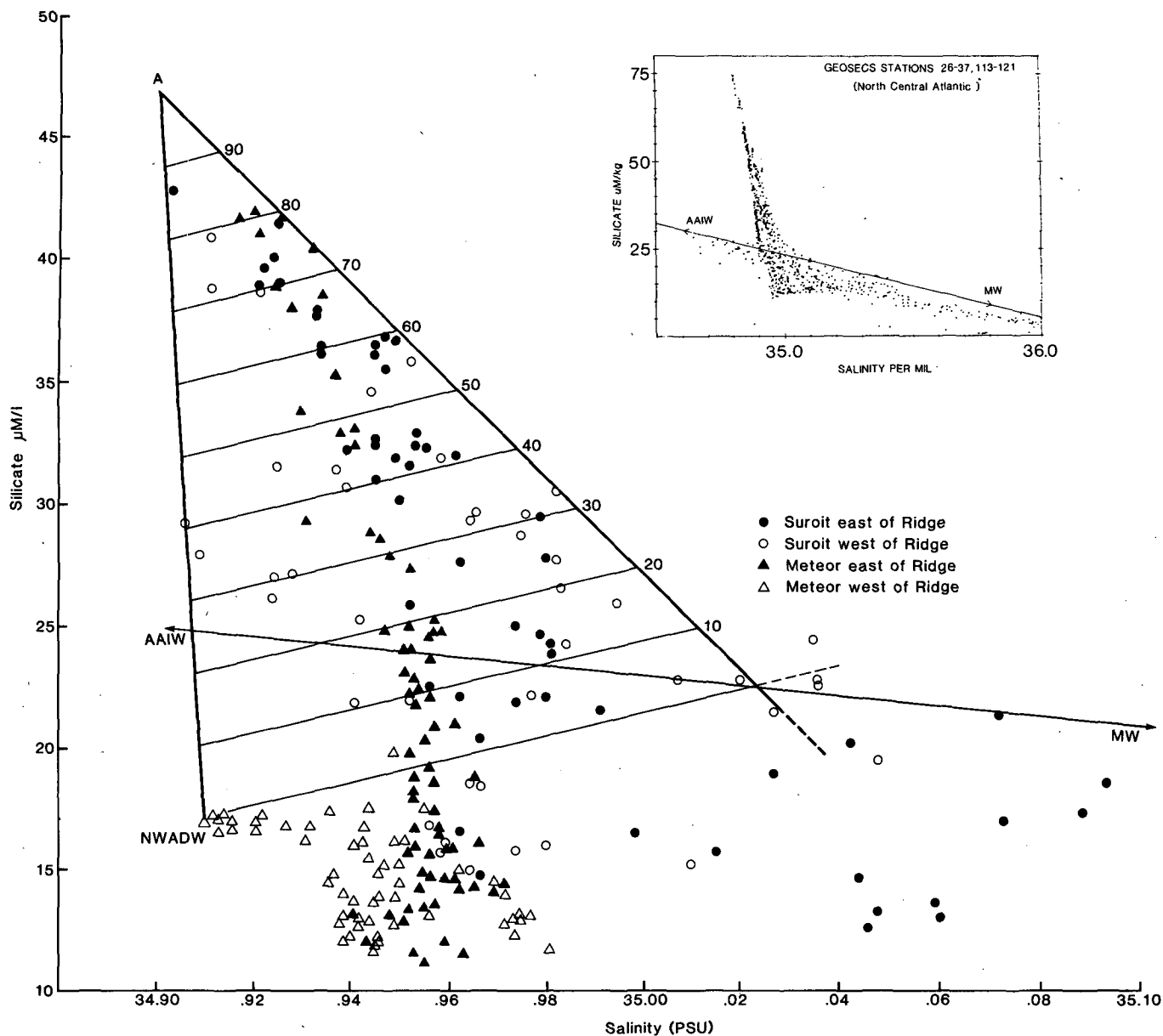FIG. 15. Dissolved oxygen vs salinity on σ_4 = 45.85.

FIG. 16. Silicate vs salinity for deep samples. The same diagram for GEOSECS stations in the North Central Atlantic is also shown.

fluence in the deep and bottom waters of the TOPO-GULF area, however, further water mass characteristics are required. Silicate is particularly useful in this respect and a salinity–silicate scatter diagram has been constructed using silicate measurements from pressures $\geq$ 2000 db (*Le Suroit*), $\geq$2400 db (*Meteor*) and corresponding CTD salinity values (Fig. 16). Two sides of a triangle can be fitted to enclose most of these data with an apex at A (silicate 46.8 μmol l^{-1}, salinity 34.899 psu) representing strong Antarctic Water (AAW) influence. NWADW, together with LSW and ISOW influences can be identified from clustering of points as shown. In order to use this diagram to assess AAW

influence quantitatively it is necessary to complete a mixing triangle with a third line along which AAW influence is taken as zero. The scatter diagram of salinity versus silicate for GEOSECS stations in the North Central Atlantic (inset) suggests at least two mixing triangles which might relate to waters in different density ranges. That for deep water clearly involves the silicate rich AAW (silicates >50 μM kg^{-1} at salinity < 34.9 psu), but the other two water types for this triangle are less well defined, while that for intermediate water appears to involve AAIW, LSW and MW; there is little evidence of mixing between AAW and either AAIW or MW.

The mixing line between AAIW and MW from the GEOSECS data has been drawn on our scatter diagram, and the third side of the triangle in Fig. 16 has been taken to extend from the extreme point attributed to NWADW (through which the first line already fitted passes) to the intersection of the second line fitted and the mixing line between AAIW and MW. Note, however, that many mixtures of water can be envisaged for which this mixing triangle would not give a correct value for AAW influence: e.g., a direct mixture of water A with either LSW or ISOW lying on the zero line in Fig. 16 would contain about 20% of water A; a mixture of AAIW and MW with salinity 34.98 psu would appear from this triangle to contain about 10% of water A. Nevertheless the results obtained from this triangle may be expected to be generally indicative of the influence of water with characteristics represented by the point A. This point does not, however, represent pure AABW. Reference to GEOSECS stations in the South Atlantic and circumpolar regions indicates that in its source region the silicate content of AABW is about 130 μM kg^{-1} (133 μmol l^{-1}) and its salinity 34.66 psu. Using the same zero line for AABW as in Fig. 16, this means that the AABW content of water with characteristics of point A is only 0.24, a factor which can be applied to the results from the mixing triangle in Fig. 16 to obtain the proportion of pure AABW present.

This has been done for stations along sections 1S–1M and 2S–2M (Fig. 17a, b). At the southern end of both sections the percentages are similar (18 to 20%), but while values in excess of 18% are found to 49°30'N at 4000 db on the eastern side of the ridge the method gives zero values for all samples north of 47°30'N on the western side and only 10% at 4000 db at 36°N. This contrast may be attributed to the presence of NWADW on the western side of the ridge with its greatest influence at about 48°N on TPG2. East of the ridge significant proportions of AABW are observed up to above 3000 m, i.e., well outside the density range of this water mass. This suggests important vertical mixing with the overlying water throughout the eastern basin, an interpretation supported by the extreme vertical homogeneity of the water below ~3000 m along TPG1 and in the southern part of TPG2 (Figs. 3, 4, 7). The tight linear θ–S relationship below 3000 m in the eastern basin south of 50°N observed by Saunders (1986), and confirmed by our data, is consistent with such deep vertical mixing in regions of AABW influence combined with strong horizontal mixing.

10. Conclusion

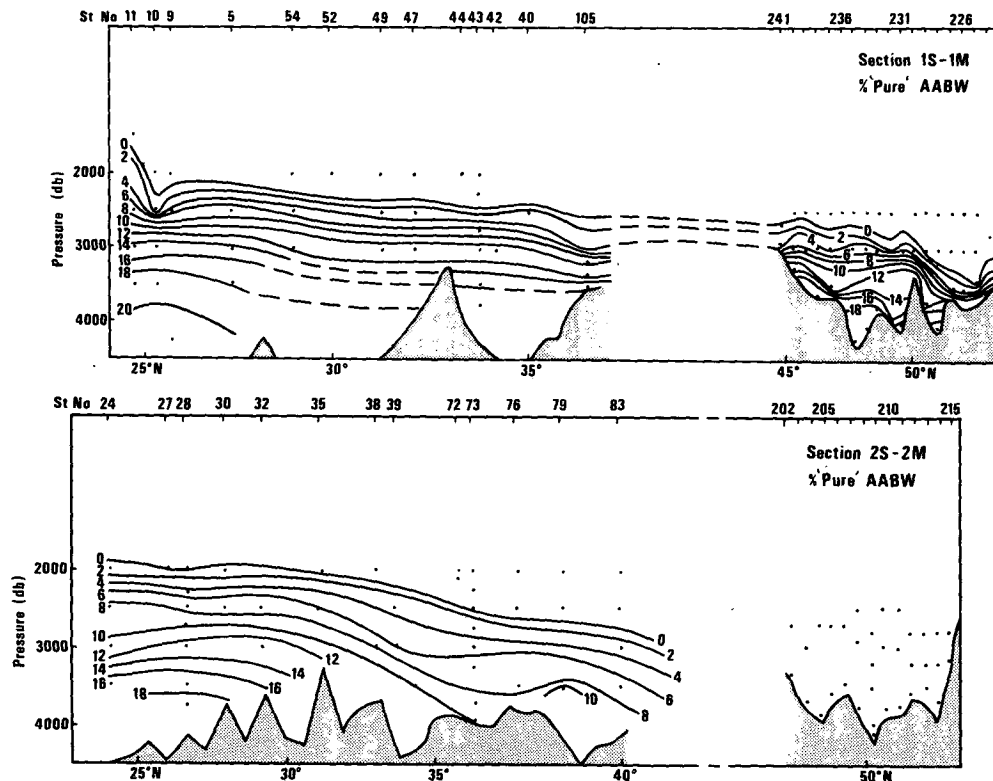For each water mass in the preceding review we pointed out those features which were either imprecise

FIG. 17. Percentage of pure Antarctic Bottom Water present in (a) section 1S–1M and (b) section 2S–2M.

or not even present in former meridional hydrographic transects, mostly because of coarser vertical and horizontal resolutions. This analysis describes, rather than explains, these features. More conclusive interpretations would require, in most cases, dedicated studies. Among these questions are:

• *The branching of the NAC.* A basic organization in two branches defined as boundaries of pure NACW in the south and outcropped SAIW in the north, with the possibility of an occasional third branch, was suggested. Such a scheme should, of course, be confronted with other data and geostrophic calculations. Even if it is confirmed, each branch is not expected to be stationary, being subject to fluctuations and meanders. East of the ridge the southern branch was shown to separate two distinct varieties (at 10° and 13°C) of McCartney and Talley's (1982) subpolar mode water. Further south the Azores Current similarly separates 18° from 13°C mode waters.

• *The circulation and mixing of SAIW.* The southward pointing tongues of SAIW observed below NACW on both sides of the ridge suggest a mean flow in the same direction, but this may be a misinterpretation. Because of an overall SW–NE orientation of the polar front the observed distribution would as well be compatible with a flow having a dominant eastward component and a negative or even slightly positive northward component. SAIW was shown to mix with NACW above, producing a modified version of NACW, and with MW in the south through strong mesoscale thermohaline variability.

• *The circulation within the subequatorial oxygen minimum.* Our sampling of this well-known feature provides further indications that it should be interpreted as the shadow zone of the ventilated thermocline model, suggesting a basically cyclonic circulation within it. AAIW influences the region from the west, but its interactions with the low oxygen anomaly which is most pronounced in the east remains unclear. Compatibility of the tracer distributions with the cyclonic circulation pattern should also be considered.

• *The vertical shear of MW and LSW distributions.* The LSW fresh anomaly is limited in our sections to ~45°N above $\sigma_2 = 36.88$, but reaches 35°N below. This vertical shear matches a similar one of the meridional MW distribution. Arhan (1987) suggested that buoyancy forcing associated with double-diffusion causes the MW shear. Were LSW a totally passive water mass it would simply fill volumes unoccupied by MW, and this interpretation would be enough. But LSW certainly has its own dynamics which must be compatible with that of the MW within the common density range.

• *The ISOW distribution in the eastern basin and behavior through the CGFZ.* To what extent ISOW spreads in the eastern basin is still uncertain. Though limited to the region west of 23°W the TOPOGULF

data suggest this water mass to have influence only north of ~50°N. South of this latitude both salinity maxima present above *and* below LSW would then be of Mediterranean origin, an a priori surprising arrangement only made possible by the wide density range of MW influence attained through double-diffusive mixing. Sampling ISOW before and after its passage through the CGFZ reveals modifications of its dynamical characteristics leading to great homogeneity at the outflow as evident from its low potential vorticity, a behavior which has not been studied to our knowledge.

• *The vertical mixing of AABW.* Our observation of a still significant proportion of pure AABW at 3000 m added to those of Saunders (1986) suggests intense cross-isopycnal mixing of this water mass with the overlying water in the eastern North Atlantic. This diagnosis conforms with the general idea that AABW having entered this basin from the south and finding no gap through which to escape in the north, can only be vertically diffused. As this water mass spreads as far as 50°N this mechanism is likely to be a major one in this oceanic basin.

REFERENCES

Arhan, M., 1987: On the large scale dynamics of the Mediterranean outflow. *Deep-Sea Res.,* **34**(7), 1187–1208.

Bainbridge, A. E., 1980: *Geosecs Atlantic Expedition. Vol. 2: Sections and profiles.* National Science Foundation.

Brewer, P. G., W. S. Broecker, W. J. Jenkins, P. B. Rhines, C. G. Rooth, J. H. Swift, T. Takahashi and R. T. Williams, 1983: A climatic freshening of the deep Atlantic north of 50°N over the past 20 years. *Science,* **222**, 1237–1239.

Bubnov, V. A., 1968: Intermediate subarctic waters in the northern part of the Atlantic Ocean. *Okeanologia,* **19**, 136–153. [English Translation (NOO Trans 545), U.S. Naval Oceanographic Office, Washington, DC, 1973.]

Harvey, J. G., 1980: Deep and bottom water in the Charlie–Gibbs fracture zone. *J. Mar. Res.,* **38**, 173–182.

——, and A. Theodorou, 1986: The circulation of Norwegian Sea overflow water in the eastern North Atlantic. *Oceanologica Acta,* **9**(4), 393–402.

Krauss, W., and R. H. Käse, 1984: Mean circulation and eddy kinetic energy in the eastern north Atlantic. *J. Geophys. Res.,* **89**, 3407–3415.

Luyten, J. R., and H. Stommel, 1986: Gyres driven by combined wind and buoyancy flux. *J. Phys. Oceanogr.,* **16**, 1551–1560.

——, J. Pedlosky and H. Stommel, 1983: The ventilated thermocline. *J. Phys. Oceanogr.,* **13**, 292–309.

McCartney, M. S., and L. D. Talley, 1982: The subpolar mode water of the North Atlantic Ocean. *J. Phys. Oceanogr.,* **12**, 1169–1188.

McDowell, S. E., 1982: Analyses of North Atlantic intermediate waters upon isopycnal surfaces and within mesoscale eddies. Ph.D. dissertation, University of Rhode Island, 227 pp.

Maillard, C., 1986: Atlas hydrographique de l'Atlantique Nord-Est. Publ. IFREMER, 133 pp.

Pollard, R. T., and S. Pu, 1985: Structure and circulation of the

Upper Atlantic Ocean northeast of the Azores. *Prog. Oceanogr.*, **14**, 443–462.

Reid, J. L., 1979: On the contribution of the Mediterranean sea outflow to the Norwegian-Greenland Sea. *Deep-Sea Res.*, **26**, 1199–1223.

—— and A. W. Mantyla, 1978: On the mid-depth circulation of the north Pacific ocean. *J. Phys. Oceanogr.*, **8**, 946–951.

Richardson, P. L., 1983: Eddy kinetic energy in the north Atlantic from surface drifters. *J. Geophys. Res.*, **88**, 4355–4367.

Roemmich, D., and C. Wunsch, 1985: Two transatlantic sections: Meridional circulation and heat flux in the subtropical North Atlantic Ocean. *Deep-Sea Res.*, **32**(6), 619–664.

Saunders, P., 1986: The accuracy of measurement of salinity, oxygen and temperature in the deep ocean. *J. Phys. Oceanogr.*, **16**, 189–195.

Schmitt, R. W., 1981: Form of the temperature–salinity relationship in the central water: Evidence for double-diffusive mixing. *J. Phys. Oceanogr.*, **11**, 1015–1026.

Smith, P. C., 1975: A streamtube model for bottom boundary currents in the ocean. *Deep-Sea Res.*, **22**, 853–873.

Sy, A., 1988: Investigation of large-scale circulation patterns in the Central North Atlantic: The North Atlantic Current, the Azores current, and the Mediterranean water plume in the area of the Mid-Atlantic ridge. *Deep-Sea Res.*, **35**, 383–413.

Talley, L. D., and M. S. McCartney, 1982: Distribution and circulation of Labrador Sea Water. *J. Phys. Oceanogr.*, **12**, 1189–1205.

Topogulf Group (The), 1986: TOPOGULF data report Vol. 1: CTD, O_2 and nutrients. Berichte aus dem Institut für Meereskunde, Nr 154, Kiel, West Germany.

Worthington, L. V., 1959: The 18° water in the Sargasso Sea. *Deep-Sea Res.*, **5**, 297–305.

——, 1972: Negative oceanic heat flux as a cause of water mass formation. *J. Phys. Oceanogr.*, **2**, 205–211.

——, 1976: On the North Atlantic circulation. Johns Hopkins Oceanographic Studies, Vol. 6, The Johns Hopkins University Press, 110 pp.

——, and W. R. Wright, 1970: *North Atlantic Ocean Atlas of Potential Temperature and Salinity in the Deep Water.* The Woods Hole Oceanographic Institution Atlas Series, Vol. 2.

Wright, W. R., and L. V. Worthington, 1970: *The Water Masses of the North Atlantic Ocean: A Volumetric Census of Temperature and Salinity.* Amer. Geophys. Soc., Serial Atlas of the Marine Environment, Vol. 19.

Wüst, G., 1935: The stratosphere of the Atlantic Ocean. Scientific results of the German Atlantic expedition of the research vessel *Meteor,* 1925–1927. Vol. 6, section 1. English translation, W. J. Emery, Ed.